Adaptive fuzzy backstepping control for attitude stabilization of flexible spacecraft with signal quantization and actuator faults

Qiuhong LIU[1], Ming LIU[2*] & Guangren DUAN[3]

[1]*Research Institute of Intelligent Control Systems, Harbin Institute of Technology, Harbin 150001, China;*
[2]*Research Center of Satellite Technology, Harbin Institute of Technology, Harbin 150001, China;*
[3]*Center for Control Theory and Guidance Technology, Harbin Institute of Technology, Harbin 150001, China*

Abstract In this study, the fault-tolerant attitude control of flexible spacecraft is investigated over digital communication channels, where a uniform quantizer is considered with respect to the sensor signals and controller indexes. Further, an adaptive fuzzy backstepping control strategy has been developed for the considered attitude stabilization issue, where the adaptive fuzzy logic method is used to approximate the rigid-flexible coupled nonlinearity of the spacecraft. In this design, the online adjusting quantizer parameters are injected into the controller gains to simultaneously compensate for the quantization errors and time-varying actuator faults. In the proposed control method, the attitude stabilization task is achieved in the presence of external disturbances, time-varying actuator faults, and signal quantization. Finally, the practical examples are compared to demonstrate the effectiveness of the proposed control strategy.

Keywords fault-tolerant control, attitude stabilization, signal quantization, adaptive fuzzy control, backstepping control

1 Introduction

During the past decades, spacecraft attitude control has become a major research topic in the aerospace domain, because it can be used to perform various advanced tasks in the aerospace domain including deep space exploration [1], space on-orbit services [2,3], and spacecraft proximity operations [4,5]. The main research issues associated with the spacecraft attitude control system design include highly nonlinear characteristics owing to the presence of rigid-flexible coupled structures [6], parameter uncertainties [7], external disturbances and actuator faults [8–11], input nonlinearity [12,13], and formation control [14–16]. During the previous decade, considerable design results have been achieved with respect to spacecraft attitude control. To name a few, a fuzzy control scheme was proposed to overcome the stochastic actuator failures and enhance the spacecraft reliability and safety [17]. A novel event-triggered sliding mode control based on periodic state measurement was initially proposed for attitude stabilization to achieve the relaxation of continuous state measurement, and the Zeno phenomenon is proved to be excluded [18]. For more relevant results, refer to [19–21]. Among the mentioned literature and other excellent research results [22–27], backstepping control and sliding mode control are considered to be the two most effective design methods because of their robustness to disturbances and uncertainties.

Networked control systems (NCSs) have attracted increasing attention because of their advantages, including low cost, convenient installation, and less weight [28]. In NCSs, the most significant features include network-induced delays [29,30], data packet losses [31,32], and signal quantization [33]. During the previous decade, plenty results have been obtained with respect to NCSs [34–41]. For instance, in [42], a novel adaptive event-triggered controller with Fourier series expansion and radial basis function neural

network (RBFNN) methods is developed to reduce the communication burden. Recently, the network communication technique has been combined with the fast-integrated technology in aerospace engineering, resulting in plug-and-play satellites. These satellites comprise independent functional modules, where data are exchanged between two modules via wireless connectors [43, 44]. Further, they exhibit several advantages, including low cost and fast integration. The plug-and-play satellites demonstrate significant application potential in modern spacecraft engineering because of its distinguished advantages, leading to increasing research attention.

Notably, in plug-and-play satellites, the measurements and command signals should be inevitably quantized during data exchange. Naturally, signal quantization refers to one of the most significant research topics for attitude tracking control of the plug-and-play satellites. The traditional spacecraft attitude control theory, which is based on the assumption that data are transmitted with infinite precision, cannot be directly applied to quantized spacecraft attitude control. Therefore, new control design methods should be designed. Various challenges are associated with the fault-tolerant flexible spacecraft control design when signal quantization is considered, which motivates this study.

In this study, we investigate the adaptive fuzzy backstepping control problem for achieving flexible spacecraft attitude stabilization. We consider dynamic and static uniform quantization schemes as the data transmission scheme, based on which the corresponding adaptive fuzzy backstepping control scheme is developed to solve the attitude stabilization problem. In this design, we propose an adaptive fuzzy approximation strategy based on the quantized attitude angle and angular velocity values for unknown nonlinear dynamics induced by rigid-flexible coupled modal vibrations. Furthermore, the proposed control scheme can completely compensate for the quantization errors and actuator faults. Finally, we present comparative examples, and the results verify the effectiveness and usefulness of the proposed control methodology.

The remainder of this paper is presented as follows. Section 2 describes the investigated design problem. The design of fuzzy backstepping control using dynamic and static quantizers is presented in Section 3. Section 4 compares the simulation results, and the conclusion is presented in Section 5.

2 Problem formulation

The spacecraft attitude kinematics equation described by a nonsingular unit quaternion is represented as follows:

$$\dot{q} = \begin{bmatrix} -\dfrac{1}{2} q_v^{\mathrm{T}} \\ \dfrac{1}{2} \left(q_0 I_3 + q_v^{\times} \right) \end{bmatrix} \Omega, \tag{1}$$

where $q = (q_0, q_v) \in \mathbb{R} \times \mathbb{R}^3$ is a unit quaternion with $q_v^{\mathrm{T}} q_v + q_0^2 = 1$, and Ω is defined as the spacecraft angular velocity. The operator $\times$ maps the vector $x = [x_1 \ x_2 \ x_3]^{\mathrm{T}} \in \mathbb{R}^3$ to its corresponding skew-symmetric matrix:

$$x^{\times} = \begin{bmatrix} 0 & -x_3 & x_2 \\ x_3 & 0 & -x_1 \\ -x_2 & x_1 & 0 \end{bmatrix}. \tag{2}$$

For flexible spacecraft with three-wheel setting, the total angular momentum is calculated as

$$H = J\Omega(t) + h + \delta^{\mathrm{T}} \dot{\eta}, \tag{3}$$

where J denotes the inertia matrix, h stands for the angular momentum vector of the reaction wheels, δ is the coupling matrix between elastic components and rigid body, and η represents the vibration mode.

For the three-reaction-wheel setting, the torque can be described as

$$\tau(t) = [\tau_1(t) \ \tau_2(t) \ \tau_3(t)]^{\mathrm{T}} = -\dot{h}, \tag{4}$$

and the partial loss of effectiveness fault can be expressed as $\tau(t) = \rho u_c$, where $u_c \in \mathbb{R}^3$ denotes the control torque command generated by the controller. The vector $\rho = \mathrm{diag}\,(\rho_1, \rho_2, \rho_3)$ stands for an unknown actuator efficiency matrix; the case of $\rho_i\,(t) = 1$ means that the ith actuator works normally, while $0 < \rho_i\,(t) < 1$ means that the ith actuator loses its effectiveness partially.
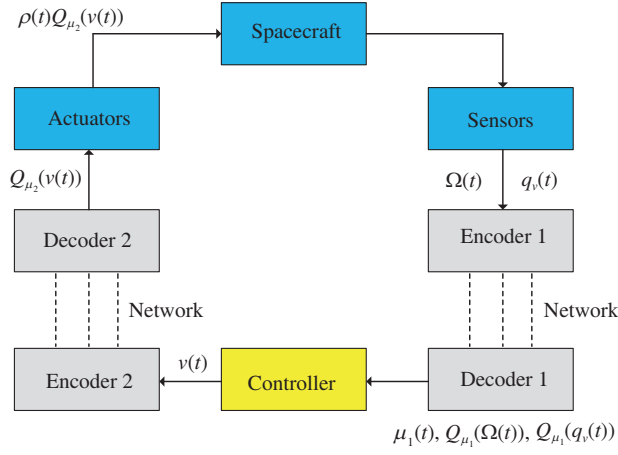
Figure 1 (Color online) Structure of the attitude control system with signal quantization.

The dynamics for flexible spacecraft under actuator faults is expressed as

$$
\begin{cases}
J\dot{\Omega} + \delta^{\mathrm{T}}\ddot{\eta} = -\Omega^{\times}\left(J\Omega + h + \delta^{\mathrm{T}}\dot{\eta}\right) + \rho u_c + d(t), \\
\ddot{\eta} + E\dot{\eta} + F\eta + \delta\dot{\Omega} = 0,
\end{cases}
\tag{5}
$$

where

$$
E = \begin{bmatrix}
2\zeta_1\Lambda_1^{\frac{1}{2}} & \cdots & 0 \\
\vdots & & \vdots \\
0 & \cdots & 2\zeta_N\Lambda_N^{\frac{1}{2}}
\end{bmatrix}, \quad
F = \begin{bmatrix}
\Lambda_1 & \cdots & 0 \\
\vdots & & \vdots \\
0 & \cdots & \Lambda_N
\end{bmatrix}
$$

are defined as the damping matrix and stiffness matrix, $\Lambda_i = \omega_{ni}^2$ with ω_{ni} referring to the natural frequency, ζ_i refers to the damping ratios, $d(t)$ represents disturbances.

Introduce an auxiliary variable $\xi = \delta\Omega + \dot{\eta}$, which derives

$$
\dot{\xi} = \delta\dot{\Omega} + \ddot{\eta} = -E\xi - E\delta\Omega - F\eta.
\tag{6}
$$

Combining Eq. (5) with (6) yields

$$
\left(J - \delta^{\mathrm{T}}\delta\right)\dot{\Omega} = -\Omega^{\times}J\Omega + \rho u_c + \Psi(\Omega, t) + d(t),
\tag{7}
$$

where $\Psi(\Omega, t)$ denotes the lumped nonlinear term as follows:

$$
\Psi(\Omega, t) = \delta^{\mathrm{T}}\left[F\ E\right]\begin{bmatrix}\eta \\ \xi\end{bmatrix} - \delta^{\mathrm{T}}E\delta\Omega - \Omega^{\times}\delta^{\mathrm{T}}\left(\xi - \delta\Omega\right) - \Omega^{\times}h.
$$

The following assumptions are necessary for the proof, achieving the attitude stabilization objective.

Assumption 1. For the efficiency factors of actuator, we suppose that $0 < \underline{\rho}_i \leqslant \rho_i \leqslant \bar{\rho}_i \leqslant 1$ with the lower and upper bounds of ρ_i being known constants, $r_1 = \min\{\underline{\rho}_i\}$, and $r_2 = \max\{\bar{\rho}_i\}$ for $i = 1, 2, 3$.

Assumption 2. The external disturbance vector $d(t) \overset{\Delta}{=} [d_1(t)\ d_2(t)\ d_3(t)]^{\mathrm{T}}$ satisfies $\|d(t)\| \leqslant \bar{d}$, where $\bar{d} \geqslant 0$ is an unknown constant.

In the following, the dynamic and static uniform quantization schemes for sensor signals and controller indexes are introduced and discussed.

As is shown in Figure 1, we consider the attitude control system structure with signal quantization, where both communication channels of sensor-controller and controller-actuator are implemented with different encoder-decoder schemes. In this setting, $Q_{\mu_1}(\cdot)$ denotes a dynamic uniform quantizer, where $\mu_1 > 0$ is updated online; $Q_{\mu_2}(\cdot)$ denotes a static uniform quantizer and $\mu_2 > 0$ is a pre-set constant value. In detail, the sensor measurements $\Omega(t)$ and $q_v(t)$ are quantized in Encoder 1 before being transmitted to the controller. Afterwards, the paired Decoder 1 at the controller side recovers the state measurements as quantized signals instead of their true values. In a similar way, the actuators receive the quantized control input command.

Remark 1. Quantizers map the true values of state signals and control commands into piecewise constants that take values in a finite quantization point set, which will inevitably induce quantization errors for measurements of attitude information and deviation of control torque. Therefore, only quantized attitude state values instead of their exact values can be used in the following design of the fuzzy logic system (FLS) and the controller, meanwhile quantization errors are of vital importance to be compensated.

We introduce the following dynamic uniform quantizer and define its belonging quantization error in such attitude control system. The dynamic uniform quantizer for any p-dimensional vector $z \in \mathbb{R}^p$ is defined as follows:

$$Q_\mu(z) = \mu \operatorname{round}\left(\frac{z}{\mu}\right), \quad \mu > 0, \tag{8}$$

where μ is a quantizer parameter which adjusts online. In addition, the quantizer error is defined as $e_z = Q_\mu(z) - z$, which satifies

$$|e_z(t)| = |Q_\mu(z) - z| \leqslant \Delta\mu, \tag{9}$$

where $\Delta = \frac{\sqrt{p}}{2}$.

Remark 2. In the research domain of quantized control systems, there exist two classical quantizers, logarithmic encoder-decoder scheme and uniform encoder-decoder scheme, respectively. The quantization resolution for logarithmic scheme becomes more precise when the original state/control signal gets closer to zero, and it becomes more coarse as the original state/control vector becomes larger, which is an appropriate characterization for practical engineering application. However, the engineering implementation of logarithmic scheme may be relatively complicated. It should be pointed out that, the dynamic uniform quantizer employed in this study also possesses the flexible adjustment for quantization sensitivity. Moreover, the dynamic uniform quantizer is easier to implement for practical engineering application.

First, for the dynamic quantizer $Q_{\mu_1}(\cdot)$ and state variable $x \in \mathbb{R}^3$, the following property holds:

$$\|x(t)\| \leqslant \|Q_{\mu_1}(x)\| + \|e_x(t)\| \leqslant \|Q_{\mu_1}(x)\| + \Delta\mu_1, \tag{10}$$

where $\Delta = \frac{\sqrt{3}}{2}$. Moreover, the following lemma relevant to the dynamic quantizer is introduced for the subsequent design.

Lemma 1 ([45]). For any given $x(t) \in \mathbb{R}^n$, and constant $0 < \vartheta < 1$, assume the parameter μ of the dynamic uniform quantizer $Q_\mu(\cdot)$ satisfies

$$\mu \leqslant \frac{\|x(t)\|}{(1 + \frac{1}{\vartheta})\Delta_n}, \tag{11}$$

where $\Delta_n = \frac{\sqrt{n}}{2}$, and then the quantization error $e_x(t)$ and $Q_{\mu_1}(x)$ satisfy the following constraints:

$$\|e_x(t)\| \leqslant \Delta_n\mu \leqslant \vartheta\|Q_{\mu_1}(x(t))\|, \tag{12}$$

$$\|Q_{\mu_1}(x(t))\| \leqslant \frac{1}{1 - \vartheta}\|x(t)\|. \tag{13}$$

Second, for static uniform quantizer $Q_{\mu_2}(\cdot)$, if the input quantization error is defined as $e_u(t) = Q_{\mu_2}(v(t)) - v(t)$, it is straightforward to obtain that

$$\|e_u(t)\| \leqslant \Delta\mu_2. \tag{14}$$

In the following discussion, our main objective is to develop an adaptive fuzzy backstepping control strategy for flexible spacecraft stabilization (1) and (7), which is capable of resolving unknown nonlinear rigid-flexible dynamics and compensating for quantization errors and actuator faults effectively.

3 Backstepping attitude control via uniform quantizer

In this section, the uniform signal quantization schemes, actuator faults, and external disturbances are considered in flexible spacecraft attitude control systems, and then an adaptive backstepping control method is proposed by employing the FLS to achieve the attitude stabilization with aforementioned factors.

3.1 Adaptive fuzzy backstepping controller design with uniform quantizer

Step 1. Define the backstepping variables as

$$x_1 = q_v, \quad x_2 = \Omega - u_\alpha, \tag{15}$$

where u_α is the virtual control to be designed later. Then, the dynamics of x_1 is

$$\dot{x}_1 = G(x_1)(x_2 + u_\alpha), \tag{16}$$

where $G(x_1) = \frac{1}{2}(\sqrt{1 - \|x_1\|^2}\mathrm{sgn}(q_0)I_3 + x_1^\times)$.

Design the virtual control as

$$u_\alpha = -k_1 x_1, \tag{17}$$

where k_1 is a positive scalar. Choose a Lyapunov function candidate

$$V_1 = x_1^{\mathrm{T}}x_1 + (1 - q_0)^2 = 2(1 - q_0). \tag{18}$$

Then the time derivative of V_1 is obtained from (18) by combining (15)–(17):

$$\dot{V}_1 = -k_1 x_1^{\mathrm{T}} x_1 + x_1^{\mathrm{T}} x_2. \tag{19}$$

Step 2. Define $J_0 = J - \delta^{\mathrm{T}}\delta$. The dynamics with respect to x_2 is

$$
\begin{aligned}
J_0 \dot{x}_2 &= -\Omega^\times J\Omega + \Psi(\Omega, t) + d(t) + u^F - J_0 \dot{u}_\alpha \\
&= -\Omega^\times J\Omega + \Psi(\Omega, t) + d(t) + u^F + k_1 J_0 G(x_1)\Omega.
\end{aligned} \tag{20}
$$

It should be pointed out that, $\Psi(\Omega, t)$ in (20) refers to a lumped nonlinear term involved with rigid-flexible dynamics, which is unaccessible to controller design. Therefore, the FLS is employed to cope with nonlinear term $\Psi(\Omega, t)$ for its approximation ability of unknown function. An FLS is generally divided into four modules: knowledge base, fuzzier, fuzzy inferencer, and defuzzifier [46].

A cluster of IF-THEN rules construct the knowledge base:

$$\text{Rule } i: \quad \text{If } b_1(t) \text{ is } F_1^i, \ b_2(t) \text{ is } F_2^i, \ldots, b_n(t) \text{ is } F_n^i,$$
$$\text{then } g(t) \text{ is } G^i, \ i = 1, 2, \ldots, N,$$

where $b(t) = [b_1(t), b_2(t), \ldots, b_n(t)]^{\mathrm{T}}$ and $g(t)$ are the FLS input and output. $\theta_{F_\iota^i}(b_\iota)$ and $\theta_{G^i}(g)$ are the membership functions relevant to fuzzy sets F_ι^i and G^i, which satisfy $\sum_{i=1}^{N}\theta_{F_\iota^i}(b_\iota) = 1$ and $\sum_{i=1}^{N}\theta_{G^i}(g) = 1$, and N denotes the number of fuzzy rules.

The FLS is given as follows based on the singleton function, center average defuzzification, and a product inference scheme:

$$g(x) = \frac{\sum_{i=1}^{N} \bar{g}_i (\Pi_{\iota=1}^{n}\theta_{F_\iota^i}(b_\iota))}{\sum_{i=1}^{N}(\Pi_{\iota=1}^{n}\theta_{F_\iota^i}(b_\iota))}, \tag{21}$$

where $\bar{g}_i$ is the point at which $\theta_{G^i}(g)$ reaches its maximum.

Fuzzy basis functions for FLS are defined as

$$\phi_i(b(t)) = \frac{\Pi_{\iota=1}^{n}\theta_{F_\iota^i}(b_\iota)}{\sum_{i=1}^{N}(\Pi_{\iota=1}^{n}\theta_{F_\iota^i}(b_\iota))}. \tag{22}$$

It is derived that by rewriting Eq. (21) over a compact set $b \in C$,

$$g(x) = \gamma^{\mathrm{T}}\phi(b(t)), \tag{23}$$

where $\phi(b) = [\phi_1(b), \phi_2(b), \ldots, \phi_N(b)]^{\mathrm{T}}$, and $\gamma = [\bar{g}_1, \bar{g}_2, \ldots, \bar{g}_N]^{\mathrm{T}}$.

However, after defining $\phi(t)$, there remains difficulties to determine appropriate $\bar{g}_i$ in (21) to achieve the minimum-approximation error. In [47], the author gives a way to adjust the optimal vector $\underline{\gamma}$ as

$$\underline{\gamma} = \arg\min_{\gamma} \left[\sup_{b \in C} \|\gamma^{\mathrm{T}}\phi(b(t)) - f(b(t))\|\right], \tag{24}$$

where $\underline{\gamma} = [\bar{g}_1^*, \bar{g}_2^*, \ldots, \bar{g}_N^*]^{\mathrm{T}}$ is the unknown optimal parameter vector.

Lemma 2 ([46]).   Supposing that $f(b(t))$ is a continuous function defined over a compact set C, there always exists an FLS as (23) with respect to arbitrary constant δ such that

$$\sup_{b \in C} |f(b(t)) - \gamma^{\mathrm{T}}\phi(b(t))| \leqslant \delta, \tag{25}$$

where δ is the ideal constant parameter.

By resorting to Lemma 2, the norm of nonlinear term $\Psi(\Omega(t))$ can be approximated based on FLS as follows:

$$\|\Psi(\Omega(t))\| = f(\Omega(t)) = \underline{\gamma}^{\mathrm{T}}\phi(\Omega(t)) + \delta_{\Psi}(t), \tag{26}$$

where $\delta_{\Psi}(t)$ denotes the minimum-approximation error of FLS.

However, the state measurement $\Omega(t)$ has been quantized through quantizer $Q_{\mu_1}(\cdot)$ before being transmitted to the controller side, and cannot be used directly in the controller design process. Hence, Eq. (26) should be modified as

$$\begin{aligned} \|\Psi(\Omega(t))\| &= \underline{\gamma}^{\mathrm{T}}\phi(\Omega(t)) + \delta_f(t) \\ &= \underline{\gamma}^{\mathrm{T}}\phi(Q_{\mu_1}(\Omega(t))) + \underline{\gamma}^{\mathrm{T}}(\phi(\Omega(t)) - \phi(Q_{\mu_1}(\Omega(t)))) + \delta_{\Psi}(t). \end{aligned} \tag{27}$$

Then, we define the reconstructed error $\delta_0(t)$ as follows:

$$\delta_0(t) = \underline{\gamma}^{\mathrm{T}}(\phi(\Omega(t)) - \phi(Q_{\mu_1}(\Omega(t)))) + \delta_{\Psi}(t), \tag{28}$$

which is assumed to maintain bounded by an unknown positive constant $\bar{\delta}_0(t)$, i.e.,

$$\|\delta_0(t)\| \leqslant \bar{\delta}_0(t). \tag{29}$$

For further analysis, it is necessary to introduce $\gamma^* = [\gamma_1^*, \gamma_2^*, \ldots, \gamma_N^*]^{\mathrm{T}}$ for $i = 1, 2, \ldots, N$ such that

$$\|\bar{g}_i^*\| \leqslant \gamma_i^*, \tag{30}$$

where γ_i^* is an unknown positive constant, and $\bar{g}_i^*$ has been mentioned in (24).

The inequality regarding of $\Psi(\Omega(t), t)$ can be derived based on aforementioned discussions:

$$\begin{aligned} \|\Psi(\Omega(t), t)\| &\leqslant \|\underline{\gamma}^{\mathrm{T}}\phi(Q_{\mu_1}(\Omega(t)))\| + \|\delta_0(t)\| \\ &\leqslant \left\| \sum_{i=1}^{N} \bar{g}_i^* \phi_i(Q_{\mu_1}(\Omega(t))) \right\| + \bar{\delta}_0. \end{aligned} \tag{31}$$

In general, Gaussian function is adopted for the basis function $\phi(t)$, so the property $\phi_i(Q_{\mu_1}(\Omega)) > 0$ holds. Consequently, it yields that

$$\left\| \sum_{i=1}^{N} \bar{g}_i^* \phi_i(Q_{\mu_1}(\Omega(t))) \right\| \leqslant \sum_{i=1}^{N} \gamma_i^* \phi_i(Q_{\mu_1}(\Omega(t))), \tag{32}$$

which further derives that

$$\|\Psi(\Omega(t), t)\| \leqslant \sum_{i=1}^{N} \gamma_i^* \phi_i(Q_{\mu_1}(\Omega(t))) + \bar{\delta}_0, \tag{33}$$

where γ_i^* and $\bar{\delta}_0$ are unknown constants to be estimated by the designed adaptive law.

Remark 3.   Due to the signal quantization behavior in sensor-controller channel, it cannot be achieved in approximating the unknown nonlinear function $\Psi(\Omega)$ by using the original value of $\Omega(t)$. Hence, a modified adaptive fuzzy logic approximation based on the quantized state values is developed.

Considering the signal quantization errors, actuator faults, and external disturbances, the following adaptive fuzzy backstepping controller is proposed to stabilize the flexible spacecraft attitude control system:

$$v(t) = -\frac{1}{r_1 - \vartheta r_2}\Bigg[(1 + \vartheta)(\|Q_{\mu_1}(x_1)\| + \Delta\mu_1) + (1 + \vartheta)\lambda_{\max}(J)(\|Q_{\mu_1}(\Omega)\| + \Delta\mu_1)^2$$

$$+ \frac{1}{2} k_1 \lambda_{\max}(J_0)(1 + \vartheta)(\|Q_{\mu_1}(\Omega)\| + \Delta\mu_1) + k_2\|Q_{\mu_1}(x_2)\| + (1 + \vartheta)r_2\Delta\mu_2$$

$$+ (1 + \vartheta)\hat{d} + (1 + \vartheta)\left(\sum_{i=1}^{N} \hat{\gamma}_i^* \phi_i(Q_{\mu_1}(\Omega))\right) + (1 + \vartheta)\hat{\delta}_0 + \varepsilon\Bigg] \frac{Q_{\mu_1}(x_2)}{\|Q_{\mu_1}(x_2)\|}, \tag{34}$$

where

$$\dot{\hat{\gamma}}_i^* = c_{\gamma_i}(1 + \vartheta)\|Q_{\mu_1}(x_2(t))\|\phi_i(Q_{\mu_1}(\Omega)), \tag{35a}$$

$$\dot{\hat{\delta}}_0 = c_\delta(1 + \vartheta)\|Q_{\mu_1}(x_2(t))\|, \tag{35b}$$

$$\dot{\hat{d}} = c_d(1 + \vartheta)\|Q_{\mu_1}(x_2(t))\|, \tag{35c}$$

and c_{γ_i}, c_δ, c_d are positive updating gains.

3.2 Stability analysis of the closed-loop system

Based on the analysis all above, the following theorem shows that the attitude control system can be stabilized by the quantized adaptive backstepping control law (34).

Theorem 1. Considering the attitude control system of flexible spacecraft (1) and (7) with (15), if the virtual control u_α is chosen as (16), and the online adjusting parameter μ_1 for quantizer Q_{μ_1} satisfies the following property

$$\mu_1 \leqslant \frac{\|x_2\|}{(1 + \frac{1}{\vartheta})\Delta}, \tag{36}$$

where the constant $0 < \vartheta \leqslant \frac{r_1}{r_2}$, then under the quantized adaptive backstepping law (34), $q_v(t)$ and $\Omega(t)$ can converge to the origin asymptotically. The initial values of adaptive variables are selected as $\hat{\gamma}_i^*(0) \geqslant 0$, $\hat{\delta}_0(0) \geqslant 0$, and $\hat{d}(0) \geqslant 0$.

Proof. First, the following error variables are defined:

$$\begin{aligned} \tilde{\gamma}_i^*(t) &= \hat{\gamma}_i^* - \gamma_i^*, \quad i = 1, 2, \ldots, N, \\ \tilde{\delta}_0(t) &= \hat{\bar{\delta}}_0 - \bar{\delta}_0, \quad \tilde{d}(t) = \hat{d} - \bar{d}. \end{aligned} \tag{37}$$

A Lyapunov candidate function can be chosen as

$$V(t) = V_1(t) + V_2(t) + V_3(t) + V_4(t) + V_5(t), \tag{38}$$

where $V_1(t)$ has been defined in (18), and

$$\begin{aligned} V_2(t) &= \frac{1}{2} x_2^{\mathrm{T}}(t) J_0 x_2(t), \quad V_3(t) = \sum_{i=1}^{N} \frac{\tilde{\gamma}_i^{*2}(t)}{2c_{\gamma_i}}, \\ V_4(t) &= \frac{\tilde{\delta}^2(t)}{2c_\delta}, \quad V_5(t) = \frac{\tilde{d}^2(t)}{2c_d}, \end{aligned} \tag{39}$$

and c_{γ_i} for $i = 1, 2, \ldots, N$, c_δ, c_d are defined in (35a).

It should be noted that the control input vector $v(t)$ is quantized via $Q_{\mu_2}(v_t)$ before reaching the actuator side, and thus the real control command executed by the actuator can be written as

$$u^F = \rho Q_{\mu_2}(v(t)) = \rho v(t) + \rho e_u(t). \tag{40}$$

Taking the quantization error into consideration, the derivative of $V_1(t)$ satisfies that

$$\dot{V}_1(t) = -k_1 x_1^{\mathrm{T}}(t)x_1(t) + x_1^{\mathrm{T}}(t)(Q_{\mu_1}(x_2(t)) - e_{x_2}(t)), \tag{41}$$

and the derivative of $V_2(t)$ satisfies that

$$\begin{aligned} \dot{V}_2(t) &= Q_{\mu_1}^{\mathrm{T}}(x_2(t))\big[-\Omega^\times(t)J\Omega(t) + \Psi(\Omega, t) + d(t) + \rho v(t) + \rho e_u(t) + k_1 J_0 G(x_1)\Omega\big] \\ &\quad - e_{x_2}^{\mathrm{T}}(t)\big[-\Omega^\times(t)J\Omega(t) + \Psi(\Omega, t) + d(t) + \rho v(t) + \rho e_u(t) + k_1 J_0 G(x_1)\Omega\big]. \end{aligned} \tag{42}$$

Along the state trajectory of attitude control system (15), it is derived that the derivative of $V(t)$ is

$$
\begin{aligned}
\dot{V}(t) = {} & -k_1 x_1^{\mathrm{T}}(t) x_1(t) + x_1^{\mathrm{T}}(t)(Q_{\mu_1}(x_2(t)) - e_{x_2}(t)) \\
& + Q_{\mu_1}^{\mathrm{T}}(x_2(t)) \big[- \Omega^{\times}(t) J \Omega(t) + \Psi(\Omega, t) + d(t) + \rho v(t) + \rho e_u(t) + k_1 J_0 G(x_1) \Omega \big] \\
& - e_{x_2}^{\mathrm{T}}(t) \big[- \Omega^{\times}(t) J \Omega(t) + \Psi(\Omega, t) + d(t) + \rho v(t) + \rho e_u(t) + k_1 J_0 G(x_1) \Omega \big] \\
& + \sum_{i=1}^{N} \frac{\tilde{\gamma}_i^*(t) \dot{\tilde{\gamma}}_i^*(t)}{c_{\gamma_i}} + \frac{\tilde{\delta}(t) \dot{\tilde{\delta}}}{c_{\delta}(t)} + \frac{\tilde{d}(t) \dot{\tilde{d}}(t)}{c_d}.
\end{aligned}
\tag{43}
$$

Recalling the quantization error of x_1 in (10), $V_1(t)$ can be enlarged as

$$
\begin{aligned}
\dot{V}_1(t) \leqslant {} & -k_1 x_1^{\mathrm{T}}(t) x_1(t) + \|x_1(t)\| \|Q_{\mu_1}(x_2(t)) - e_{x_2}(t)\| \\
\leqslant {} & -k_1 x_1^{\mathrm{T}}(t) x_1(t) + (\|Q_{\mu_1}(x_1(t))\| + \Delta\mu_1) \|e_{x_2}(t)\| + (\|Q_{\mu_1}(x_1(t))\| + \Delta\mu_1) \|Q_{\mu_1}(x_2(t))\|.
\end{aligned}
\tag{44}
$$

On the other hand, the term $Q_{\mu_1}^{\mathrm{T}}(x_2(t))(-\Omega^{\times}(t) J \Omega(t))$ can be enlarged as

$$
\begin{aligned}
Q_{\mu_1}^{\mathrm{T}}(x_2)(-\Omega^{\times} J \Omega) \leqslant {} & \|Q_{\mu_1}(x_2)\| \lambda_{\max}(J) \|\Omega\|^2 \\
\leqslant {} & \|Q_{\mu_1}(x_2)\| \lambda_{\max}(J)(\|Q_{\mu_1}(\Omega)\| + \Delta\mu_1)^2.
\end{aligned}
\tag{45}
$$

Considering the modified FLS expressed in (33), it yields that

$$
Q_{\mu_1}^{\mathrm{T}}(x_2) \Psi(\Omega, t) \leqslant \|Q_{\mu_1}(x_2)\| \sum_{i=1}^{N} \gamma_i^* \phi(Q_{\mu_1}(\Omega)) + \|Q_{\mu_1}(x_2)\| \bar{\delta}_0.
\tag{46}
$$

By Assumption 2, it is derived that

$$
Q_{\mu_1}^{\mathrm{T}}(x_2) d(t) \leqslant \|Q_{\mu_1}(x_2)\| \bar{d}.
\tag{47}
$$

It should be noted that $\lambda_{\max}(G(x_1)) \leqslant \frac{1}{2}$ for $x_1 \in \mathbb{R}^3$, and then it is derived as

$$
Q_{\mu_1}^{\mathrm{T}}(x_2)(-k_1 J_0 G(x_1) \Omega) \leqslant \frac{1}{2} k_1 \lambda_{\max}(J_0) \|Q_{\mu_1}(x_2)\| (\|Q_{\mu_1}(\Omega)\| + \Delta\mu_1).
\tag{48}
$$

Recalling the input quantization error in (14), the following inequality holds:

$$
Q_{\mu_1}^{\mathrm{T}}(x_2) \rho e_u(t) \leqslant \|Q_{\mu_1}(x_2)\| \Delta\mu_2.
\tag{49}
$$

By Assumption 1, $r_1 < \lambda(\rho) < r_2$ can be obtained, where r_1, r_2 are known constants which refer to actuator efficiency bounds. Thus the following term can be enlarged as

$$
\begin{aligned}
& Q_{\mu_1}^{\mathrm{T}}(x_2(t)) \big[- \Omega^{\times}(t) J \Omega(t) + \Psi(\Omega, t) + d(t) + \rho v(t) + \rho e_u(t) + k_1 J_0 G(x_1) \Omega \big] \\
& \leqslant \|Q_{\mu_1}(x_2(t))\| \Bigg[\lambda_{\max}(J)(\|Q_{\mu_1}(\Omega)\| + \Delta\mu_1)^2 + \frac{1}{2} k_1 \lambda_{\max}(J_0)(\|Q_{\mu_1}(\Omega)\| + \Delta\mu_1) + \bar{d} \\
& \quad + \sum_{i=1}^{N} \gamma_i^* \phi(Q_{\mu_1}(\Omega)) + \bar{\delta}_0 + r_2 \Delta\mu_2 \Bigg] + Q_{\mu_1}^{\mathrm{T}}(x_2(t)) \rho v(t).
\end{aligned}
\tag{50}
$$

Considering the state quantization error $e_{x2}(t)$ in (43), it can be seen that $e_{x2}(t)$ is coupled with state variables, unknown nonlinearity function, external disturbances, and control input, which makes it complex to eliminate the effects of both state quantization and input quantization behavior. Therefore, we should focus on the characteristics of both dynamic quantizer Q_{μ_1} and static quantizer Q_{μ_2}. According to Lemma 1, the norm of $e_{x2}(t)$ and x_2 follow the constraint:

$$
\|e_{x_2}(t)\| \leqslant \vartheta \|Q_{\mu_1}(x_2(t))\|.
\tag{51}
$$

Hence, it is easy to obtain the following inequality

$$
-e_{x_2}^{\mathrm{T}}(t) \big[- \Omega^{\times}(t) J \Omega(t) + \Psi(\Omega, t) + d(t) + \rho v(t) + \rho e_u(t) + k_1 J_0 G(x_1) \Omega \big]
$$

$$
\leqslant \vartheta \|Q_{\mu_1}(x_2(t))\| \left[\lambda_{\max}(J)(\|Q_{\mu_1}(\Omega)\| + \Delta\mu_1)^2 + \frac{1}{2}k_1\lambda_{\max}(J_0)(\|Q_{\mu_1}(\Omega)\| + \Delta\mu_1) + \bar{d} \right.
$$

$$
\left. + \sum_{i=1}^{N} \gamma_i^* \phi(Q_{\mu_1}(\Omega)) + \bar{\delta}_0 + r_2\Delta\mu_2 \right] - e_{x_2}^{\mathrm{T}}(t)\rho v(t). \tag{52}
$$

Then considering the coupled term $-e_{x_2}^{\mathrm{T}}(t)\rho v(t)$ with $v(t)$ designed in (34), it is derived that

$$
- e_{x_2}^{\mathrm{T}}(t)\rho v(t) \leqslant \frac{\vartheta r_2}{r_1 - \vartheta r_2}\|Q_{\mu_1}(x_2(t))\| \left[(1+\vartheta)(\|Q_{\mu_1}(x_1)\| + \Delta\mu_1) \right.
$$

$$
+ (1+\vartheta)\lambda_{\max}(J)(\|Q_{\mu_1}(\Omega)\| + \Delta\mu_1)^2
$$

$$
+ \frac{1}{2}k_1\lambda_{\max}(J_0)(1+\vartheta)(\|Q_{\mu_1}(\Omega)\| + \Delta\mu_1)
$$

$$
+ k_2\|Q_{\mu_1}(x_2)\| + (1+\vartheta)r_2\Delta\mu_2 + (1+\vartheta)\hat{d}
$$

$$
\left. + (1+\vartheta)\left(\sum_{i=1}^{N} \hat{\gamma}_i^* \phi_i(Q_{\mu_1}(\Omega)) \right) + (1+\vartheta)\hat{\delta}_0 + \varepsilon \right], \tag{53}
$$

which further implies that

$$
-e_{x_2}^{\mathrm{T}}(t)\big[-\Omega^{\times}(t)J\Omega(t) + \Psi(\Omega,t) + d(t) + \rho v(t) + \rho e_u(t) + k_1 J_0 G(x_1)\Omega \big]
$$

$$
\leqslant \vartheta \|Q_{\mu_1}(x_2(t))\| \left[\lambda_{\max}(J)(\|Q_{\mu_1}(\Omega)\| + \Delta\mu_1)^2 + \frac{1}{2}k_1\lambda_{\max}(J_0)(\|Q_{\mu_1}(\Omega)\| + \Delta\mu_1) + \bar{d} \right.
$$

$$
\left. + \sum_{i=1}^{N} \gamma_i^* \phi(Q_{\mu_1}(\Omega)) + \bar{\delta}_0 + r_2\Delta\mu_2 \right]
$$

$$
+ \frac{\vartheta r_2}{r_1 - \vartheta r_2}\|Q_{\mu_1}(x_2(t))\| \left[(1+\vartheta)(\|Q_{\mu_1}(x_1)\| + \Delta\mu_1) + (1+\vartheta)\lambda_{\max}(J)(\|Q_{\mu_1}(\Omega)\| + \Delta\mu_1) \right.
$$

$$
+ \frac{1}{2}\lambda_{\max}(J_0)(1+\vartheta)(\|Q_{\mu_1}(\Omega)\| + \Delta\mu_1)^2 + k_2\|Q_{\mu_1}(x_2)\| + (1+\vartheta)r_2\Delta\mu_2 + (1+\vartheta)\hat{d}
$$

$$
\left. + (1+\vartheta)\left(\sum_{i=1}^{N} \hat{\gamma}_i^* \phi_i(Q_{\mu_1}(\Omega)) \right) + (1+\vartheta)\hat{\delta}_0 + \varepsilon \right], \tag{54}
$$

where ϑ is designed to satisfy $\vartheta < \frac{r_1}{r_2}$.

Based on the above analysis, it follows that

$$
\dot{V}(t) \leqslant -k_1 x_1^{\mathrm{T}}(t)x_1(t) + (\|Q_{\mu_1}(x_1(t))\| + \Delta\mu_1)\|Q_{\mu_1}(x_2(t))\| + (\|Q_{\mu_1}(x_1(t))\| + \Delta\mu_1)\vartheta\|Q_{\mu_1}(x_2(t))\|
$$

$$
+ \|Q_{\mu_1}(x_2(t))\| \left[\lambda_{\max}(J)(\|Q_{\mu_1}(\Omega)\| + \Delta\mu_1)^2 + \frac{1}{2}k_1\lambda_{\max}(J_0)(\|Q_{\mu_1}(\Omega)\| + \Delta\mu_1) + \bar{d} \right.
$$

$$
\left. + \sum_{i=1}^{N} \gamma_i^* \phi(Q_{\mu_1}(\Omega)) + \bar{\delta}_0 + r_2\Delta\mu_2 \right] + Q_{\mu_1}^{\mathrm{T}}(x_2(t))\rho v(t)
$$

$$
+ \vartheta \|Q_{\mu_1}(x_2(t))\| \left[\lambda_{\max}(J)(\|Q_{\mu_1}(\Omega)\| + \Delta\mu_1)^2 + \frac{1}{2}k_1\lambda_{\max}(J_0)(\|Q_{\mu_1}(\Omega)\| + \Delta\mu_1) + \bar{d} \right.
$$

$$
\left. + \sum_{i=1}^{N} \gamma_i^* \phi(Q_{\mu_1}(\Omega)) + \bar{\delta}_0 + r_2\Delta\mu_2 \right]
$$

$$
+ \frac{\vartheta r_2}{r_1 - \vartheta r_2}\|Q_{\mu_1}(x_2(t))\| \left[(1+\vartheta)(\|Q_{\mu_1}(x_1)\| + \Delta\mu_1) + (1+\vartheta)\lambda_{\max}(J)(\|Q_{\mu_1}(\Omega)\| + \Delta\mu_1) \right.
$$

$$
+ \frac{1}{2}\lambda_{\max}(J_0)(1+\vartheta)(\|Q_{\mu_1}(\Omega)\| + \Delta\mu_1)^2 + k_2\|Q_{\mu_1}(x_2)\| + (1+\vartheta)r_2\Delta\mu_2 + (1+\vartheta)\hat{d}
$$

$$+ (1 + \vartheta) \left(\sum_{i=1}^{N} \hat{\gamma}_i^* \phi_i(Q_{\mu_1}(\Omega)) \right) + (1 + \vartheta)\hat{\delta}_0 + \varepsilon \Bigg]$$

$$+ \sum_{i=1}^{N} \frac{\tilde{\gamma}_i^*(t)\dot{\hat{\gamma}}_i^*(t)}{c_{\gamma_i}} + \frac{\tilde{\delta}(t)\dot{\hat{\delta}}}{c_\delta(t)} + \frac{\tilde{d}(t)\dot{\hat{d}}(t)}{c_d}. \tag{55}$$

Substituting the control law into the term $Q_{\mu_1}^{\mathrm{T}}(x_2)\rho v(t)$, it yields that

$$Q_{\mu_1}^{\mathrm{T}}(x_2)\rho v(t)$$

$$\leqslant \left(-\|Q_{\mu_1}(x_2(t))\| - \frac{\vartheta r_2}{r_1 - \vartheta r_2}\|Q_{\mu_1}(x_2(t))\| \right) \times \Bigg[(1 + \vartheta)(\|Q_{\mu_1}(x_1)\| + \Delta\mu_1)$$

$$+ (1 + \vartheta)\lambda_{\max}(J)(\|Q_{\mu_1}(\Omega)\| + \Delta\mu_1)^2 + \frac{1}{2}k_1\lambda_{\max}(J_0)(1 + \vartheta)(\|Q_{\mu_1}(\Omega)\| + \Delta\mu_1)$$

$$+ k_2\|Q_{\mu_1}(x_2)\| + (1 + \vartheta)r_2\Delta\mu_2 + (1 + \vartheta)\hat{d} + (1 + \vartheta)\left(\sum_{i=1}^{N} \hat{\gamma}_i^* \phi_i(Q_{\mu_1}(\Omega)) \right) + (1 + \vartheta)\hat{\delta}_0 + \varepsilon \Bigg]. \tag{56}$$

Thus, $V_2(t)$ follows the following property:

$$\dot{V}_2(t) = Q_{\mu_1}^{\mathrm{T}}(x_2(t))\big[-\Omega^\times(t)J\Omega(t) + \Psi(\Omega,t) + d(t) + \rho v(t) + \rho e_u(t) + k_1 J_0 G(x_1)\Omega \big]$$

$$-e_{x_2}^{\mathrm{T}}(t)\big[-\Omega^\times(t)J\Omega(t) + \Psi(\Omega,t) + d(t) + \rho v(t) + \rho e_u(t) + k_1 J_0 G(x_1)\Omega \big]$$

$$\leqslant \|Q_{\mu_1}(x_2(t))\| \Bigg[\lambda_{\max}(J)(\|Q_{\mu_1}(\Omega)\| + \Delta\mu_1)^2 + \frac{1}{2}k_1\lambda_{\max}(J_0)(\|Q_{\mu_1}(\Omega)\| + \Delta\mu_1) + \bar{d}$$

$$+ \sum_{i=1}^{N} \gamma_i^* \phi(Q_{\mu_1}(\Omega)) + \bar{\delta}_0 + r_2\Delta\mu_2 \Bigg]$$

$$+ \vartheta\|Q_{\mu_1}(x_2(t))\| \Bigg[\lambda_{\max}(J)(\|Q_{\mu_1}(\Omega)\| + \Delta\mu_1)^2 + \frac{1}{2}k_1\lambda_{\max}(J_0)(\|Q_{\mu_1}(\Omega)\| + \Delta\mu_1) + \bar{d}$$

$$+ \sum_{i=1}^{N} \gamma_i^* \phi(Q_{\mu_1}(\Omega)) + \bar{\delta}_0 + r_2\Delta\mu_2 \Bigg]$$

$$+ \frac{\vartheta r_2}{r_1 - \vartheta r_2}\|Q_{\mu_1}(x_2(t))\| \Bigg[(1 + \vartheta)(\|Q_{\mu_1}(x_1)\| + \Delta\mu_1) + (1 + \vartheta)\lambda_{\max}(J)(\|Q_{\mu_1}(\Omega)\| + \Delta\mu_1)$$

$$+ \frac{1}{2}\lambda_{\max}(J_0)(1 + \vartheta)(\|Q_{\mu_1}(\Omega)\| + \Delta\mu_1)^2 + k_2\|Q_{\mu_1}(x_2)\| + (1 + \vartheta)r_2\Delta\mu_2 + (1 + \vartheta)\hat{d}$$

$$+ (1 + \vartheta)\left(\sum_{i=1}^{N} \hat{\gamma}_i^* \phi_i(Q_{\mu_1}(\Omega)) \right) + (1 + \vartheta)\hat{\delta}_0 + \varepsilon \Bigg]$$

$$- \|Q_{\mu_1}(x_2(t))\| \Bigg[(1 + \vartheta)(\|Q_{\mu_1}(x_1)\| + \Delta\mu_1) + (1 + \vartheta)\lambda_{\max}(J)(\|Q_{\mu_1}(\Omega)\| + \Delta\mu_1)^2$$

$$+ \frac{1}{2}k_1\lambda_{\max}(J_0)(1 + \vartheta)(\|Q_{\mu_1}(\Omega)\| + \Delta\mu_1) + k_2\|Q_{\mu_1}(x_2)\| + (1 + \vartheta)r_2\Delta\mu_2 + (1 + \vartheta)\hat{d}$$

$$+ (1 + \vartheta)\left(\sum_{i=1}^{N} \hat{\gamma}_i^* \phi_i(Q_{\mu_1}(\Omega)) \right) + (1 + \vartheta)\hat{\delta}_0 + \varepsilon \Bigg]$$

$$- \frac{\vartheta r_2}{r_1 - \vartheta r_2}\|Q_{\mu_1}(x_2(t))\| \Bigg[(1 + \vartheta)(\|Q_{\mu_1}(x_1)\| + \Delta\mu_1) + (1 + \vartheta)\lambda_{\max}(J)(\|Q_{\mu_1}(\Omega)\| + \Delta\mu_1)^2$$

$$+ \frac{1}{2}k_1\lambda_{\max}(J_0)(1 + \vartheta)(\|Q_{\mu_1}(\Omega)\| + \Delta\mu_1) + k_2\|Q_{\mu_1}(x_2)\| + (1 + \vartheta)r_2\Delta\mu_2 + (1 + \vartheta)\hat{d}$$

$$+ (1 + \vartheta)\left(\sum_{i=1}^{N} \hat{\gamma}_i^* \phi_i(Q_{\mu_1}(\Omega)) \right) + (1 + \vartheta)\hat{\delta}_0 + \varepsilon \Bigg], \tag{57}$$

which further implies that

$$
\begin{aligned}
\dot{V}_2(t) \leqslant{} & -\|Q_{\mu_1}(x_2(t))\|(1+\vartheta)(\|Q_{\mu_1}(x_1(t))\| + \Delta\mu_1) - (1+\vartheta)\|Q_{\mu_1}(x_2(t))\|\tilde{d} \\
& -(1+\vartheta)\|Q_{\mu_1}(x_2(t))\|\left(\sum_{i=1}^{N}\tilde{\gamma}_i\phi_i(Q_{\mu_1}(\Omega))\right) - (1+\vartheta)\|Q_{\mu_1}(x_2(t))\|\tilde{\delta}_0 \\
& -(k_2+\varepsilon)\|Q_{\mu_1}(x_2(t))\|^2.
\end{aligned}
\tag{58}
$$

Noting that $\dot{\tilde{\gamma}}_i^*(t) = \dot{\hat{\gamma}}_i^*(t)$, $\dot{\tilde{\delta}}_0(t) = \dot{\hat{\delta}}_0(t)$, and $\dot{\tilde{d}}(t) = \dot{\hat{d}}(t)$, it follows from the adaptive law that

$$
\begin{aligned}
\dot{V}(t) &= -\dot{V}_1(t) + \dot{V}_2(t) + \dot{V}_3(t) + \dot{V}_4(t) + \dot{V}_5(t) \\
&\leqslant -k_1 x_1^{\mathrm{T}}(t)x_1(t) - (k_2+\varepsilon)\|Q_{\mu_1}(x_2(t))\|^2 \\
&\leqslant -k_1 x_1^{\mathrm{T}}(t)x_1(t) - \frac{(k_2+\varepsilon)}{1-\vartheta}x_2^{\mathrm{T}}(t)x_2(t).
\end{aligned}
\tag{59}
$$

It can be seen that $\dot{V}(t) < 0$ for $x_1(t) \neq 0$ and $x_2(t) \neq 0$, so the states $x_1(t)$ and $x_2(t)$ will converge to zero under the designed controller, which further implies that $q_v(t)$ and $\Omega(t)$ will converge to zero, and $q_0(t)$ converges to 1. Thus the proof is completed.

Remark 4. The selecting conditions for initial values are given as $\hat{\gamma}_i^*(0) \geqslant 0$, $\hat{\delta}_0(0) \geqslant 0$, and $\hat{d}(0) \geqslant 0$. By the adaptive laws (35a)–(35c), it can be guaranteed that $\hat{\gamma}_i^*(t)$, $\hat{\delta}_0(t)$, and $\hat{d}(t)$ are positive values during the controller activation time. It is also noted that the positive constraints of $\hat{\gamma}_i^*(t)$, $\hat{\delta}_0(t)$, and $\hat{d}(t)$ are essential conditions for stability analysis procedure. In practical engineering application, to avoid overestimation of adaptive variables, the monotone increasing adaptive laws (35a)–(35c) can be terminated when tracking errors converge into a small residual set in the vicinity of origin.

4   Simulation results

In this section, a practical example is presented to verify the effectiveness of the quantized fault-tolerant control strategy proposed in this study, and a comparative example with traditional adaptive fast sliding mode control (AFSMC) method is also presented to show the superiority of the developed control method. The spacecraft parameters used in [48] are employed. The inertia matrix and the coupling matrix are given by

$$
J = \begin{bmatrix} 350 & 3 & 4 \\ 3 & 280 & 10 \\ 4 & 10 & 190 \end{bmatrix} \text{kgm}^2, \qquad \delta = \begin{bmatrix} 6.45637 & 1.27814 & 2.15629 \\ -1.25619 & 0.91756 & -1.67264 \\ 1.11687 & 2.48901 & -0.83674 \\ 1.23637 & -2.6581 & -1.12503 \end{bmatrix}.
$$

For flexible appendages, the natural frequencies are given by $\omega_{n1} = 0.7681$ rad/s, $\omega_{n2} = 1.1038$ rad/s, $\omega_{n3} = 1.8733$ rad/s, $\omega_{n4} = 2.5496$ rad/s, and the damping ratios are given by $\zeta_1 = 0.005607$, $\zeta_2 = 0.008620$, $\zeta_3 = 0.01283$, $\zeta_4 = 0.02516$.

We consider the spacecraft is serving under the following working conditions:

(I) The initial attitude of the spacecraft is chosen as roll angle $8°$, pitch angle $-5°$, yaw angle $-12°$, which corresponds to the quaternion $q(0) = [0.9915 \ 0.0648 \ -0.0506 \ -0.1011]^{\mathrm{T}}$; the initial angular velocity of the satellite is $\Omega_x(0) = -0.8°$/s, $\Omega_y(0) = 0.5°$/s, $\Omega_z(0) = 1.5°$/s; the initial vibration mode $\eta_i(0) = 0.001$, and its derivative $\dot{\eta}_i(0) = 0.0005$.

(II) The external disturbances are given by

$$
d = \begin{bmatrix} -3 + 2\Omega_1\sin(0.11t) - \cos(0.4\pi t) + 4\cos(0.2\pi t) \\ 4 + \Omega_2\cos(0.11t) - 2\cos(0.4\pi t) + 3\sin(0.2\pi t) \\ -3 - 2\Omega_3\cos(0.11t) - 3\sin(0.4\pi t) + 4\sin(0.2\pi t) \end{bmatrix} \times 10^{-4} \text{ Nm}.
$$

(III) The bounds of the actuator efficiency factor $\rho_i(t)$ are set as $r_1 = \underline{\rho}_i = 0.45$ and $r_2 = \bar{\rho}_i = 1$. The time-varying efficiency factors of the actuators are given by

$$
\rho_1(t) = 0.8 - 0.1\sin(5t), \quad \rho_2(t) = 0.67, \quad \rho_3(t) = 0.75 + 0.1\cos(2t).
$$
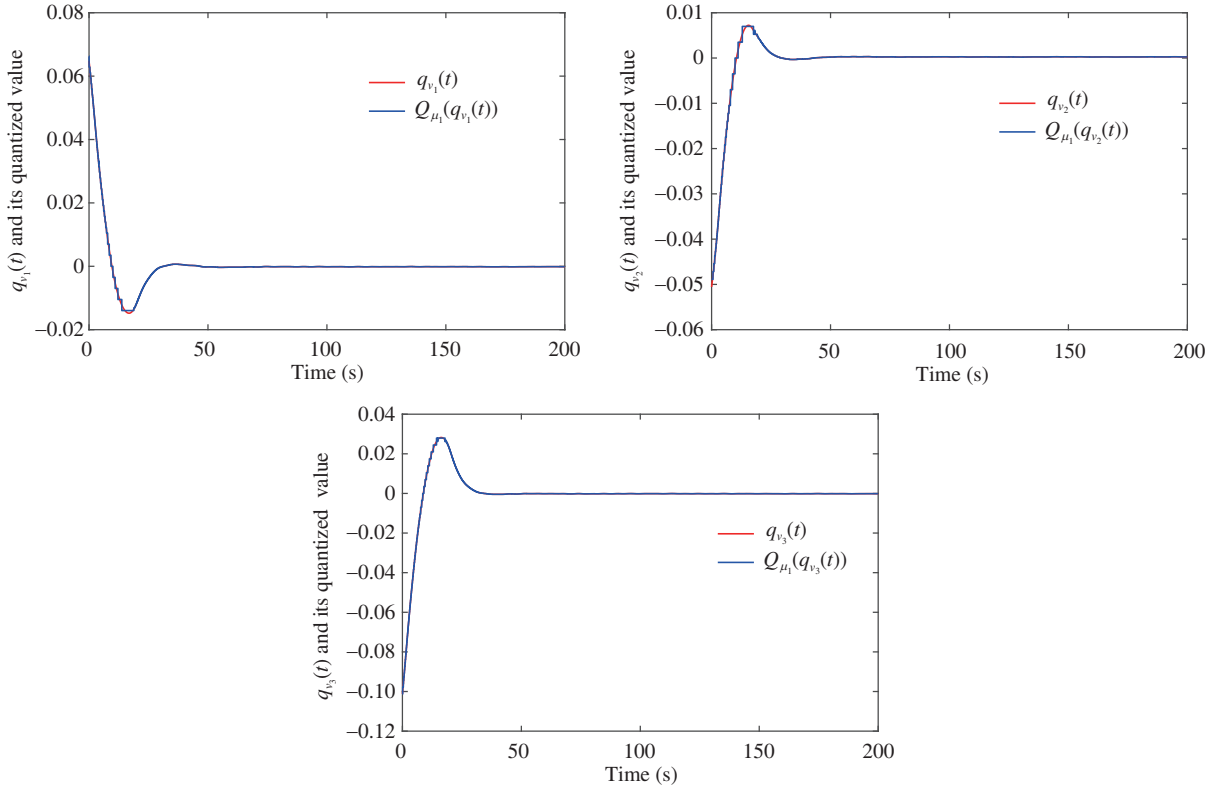
Figure 2 (Color online) Quaternion values and their quantized values under the proposed controller.

(IV) For dynamic uniform quantizer Q_{μ_1}, the co-design parameters are selected as $\vartheta = 0.24$ and $\Delta = \frac{\sqrt{3}}{2}$, and then the online adjusting parameter is tuned by $\mu_1(t) = \frac{\|x_2(t)\|}{(1+\frac{1}{\vartheta})\Delta}$. For static uniform quantizer Q_{μ_2}, the quantization resolution parameter is set as $\Delta = \frac{\sqrt{3}}{2}$, $\mu_2 = 0.005$.

(V) Moreover, in order to make the simulation more practical, the input saturation is considered. For reaction wheels, the maximum output torque and angular momentum are $\tau_{\max} = 0.5$ Nm and $h_{\max} = 10$ Nms, respectively.

4.1 Control performance under the proposed control scheme

In this subsection, the simulation is implemented with the proposed method, and the controller parameters for attitude control is selected as follows. First, define the fuzzy membership functions as follows:

$$\theta_{F_\iota^i}(\Omega_\iota) = \mathrm{e}^{-(\Omega_\iota+(3-i)/10)^2/0.3}, \ \iota \in \{1,2,3\}, \ i \in \{1,2,3,4,5\},$$

which is known to the controller. Furthermore, it derives that

$$\phi_i(\Omega(t)) = \frac{\Pi_{\iota=1}^3 \theta_{F_\iota^i}(\Omega_\iota)}{\sum_{i=1}^5 (\Pi_{\iota=1}^3 \theta_{F_\iota^i}(\Omega_\iota))}.$$

Second, the adaptive gains for $\hat{\delta}_0$, $\hat{d}$, and $\hat{\gamma}_i^*$, $i = 1, 2, 3$ are chosen as $c_\delta = 0.001$, $c_d = 0.0035$, $c_{\gamma_1} = 5$, $c_{\gamma_2} = 0.5$, $c_{\gamma_3} = 0.5$, $c_{\gamma_4} = 0.5$, $c_{\gamma_5} = 5$, respectively, the scalar ε is set as 0.01, and the backstepping control law gains are set as $k_1 = 0.375$, $k_2 = 145$.

Third, the initial values of adaptive variables are $\hat{\gamma}_i(0) = 0$, $i = 1, 2, 3, 4, 5$, $\hat{\delta}(0) = 0$, and $\hat{d}(0) = 0$.

To prevent the control signals from chattering, we employ $\frac{Q_{\mu_1}(x_2(t))}{\|Q_{\mu_1}(x_2(t))\|+0.0015}$ to realize the term $\frac{Q_{\mu_1}(x_2(t))}{\|Q_{\mu_1}(x_2(t))\|}$ in the simulation.

Under the quantized adaptive backstepping control law (34), the simulation results are shown in Figures 2–5 clearly. Figures 2 and 3 present the quaternion values and angular velocity values with their quantized values of the closed-loop flexible spacecraft control system respectively, which show that
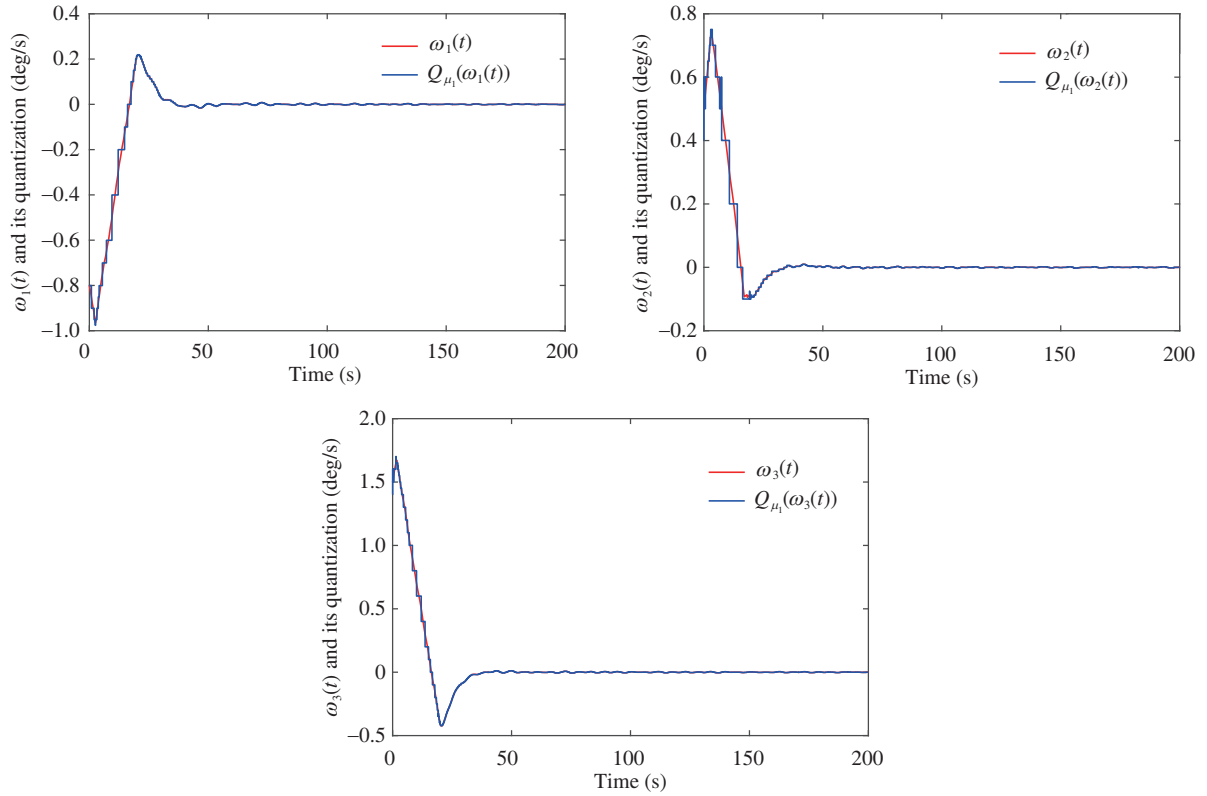
Figure 3 (Color online) Angular velocity values and their quantized values under the proposed controller.
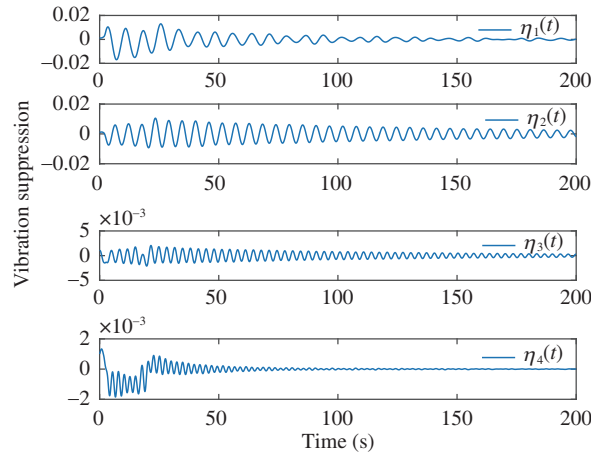
Figure 4 (Color online) The curve of vibration mode under the proposed controller.

the proposed method can compensate for the quantized errors completely. Figure 4 presents the vibration displacements, which are all suppressed in bounded range. Figure 5 presents the quantized control torque commands generated by the proposed controller, and Figure 6 gives the momentum of reaction wheel actuators.

4.2 Control performance under the existing AFSMC method

In this subsection, the traditional AFSMC [49] is employed under actuator faults and signal quantization to make a comparison with the proposed method in this study. The controller parameters are adopted as they were in [49]. Figures 7 and 8 illustrate the quaternion and angular velocity of the spacecraft during the attitude stabilization process.
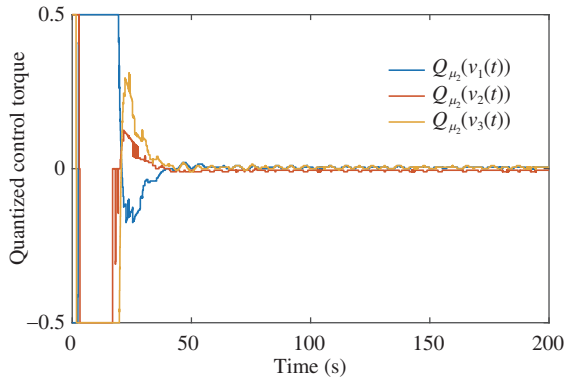
Figure 5 (Color online) The curve of quantized control torque under the proposed controller.
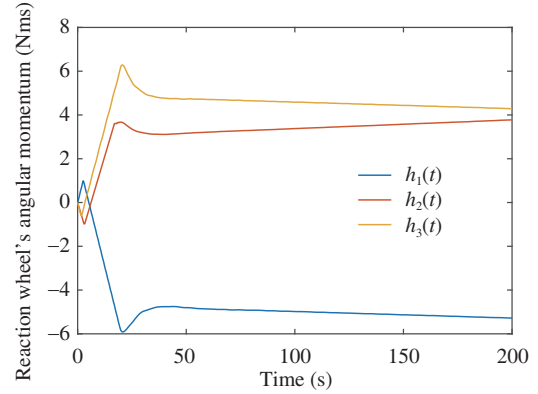
Figure 6 (Color online) The curve of reaction wheel's angular momentum under the proposed controller.
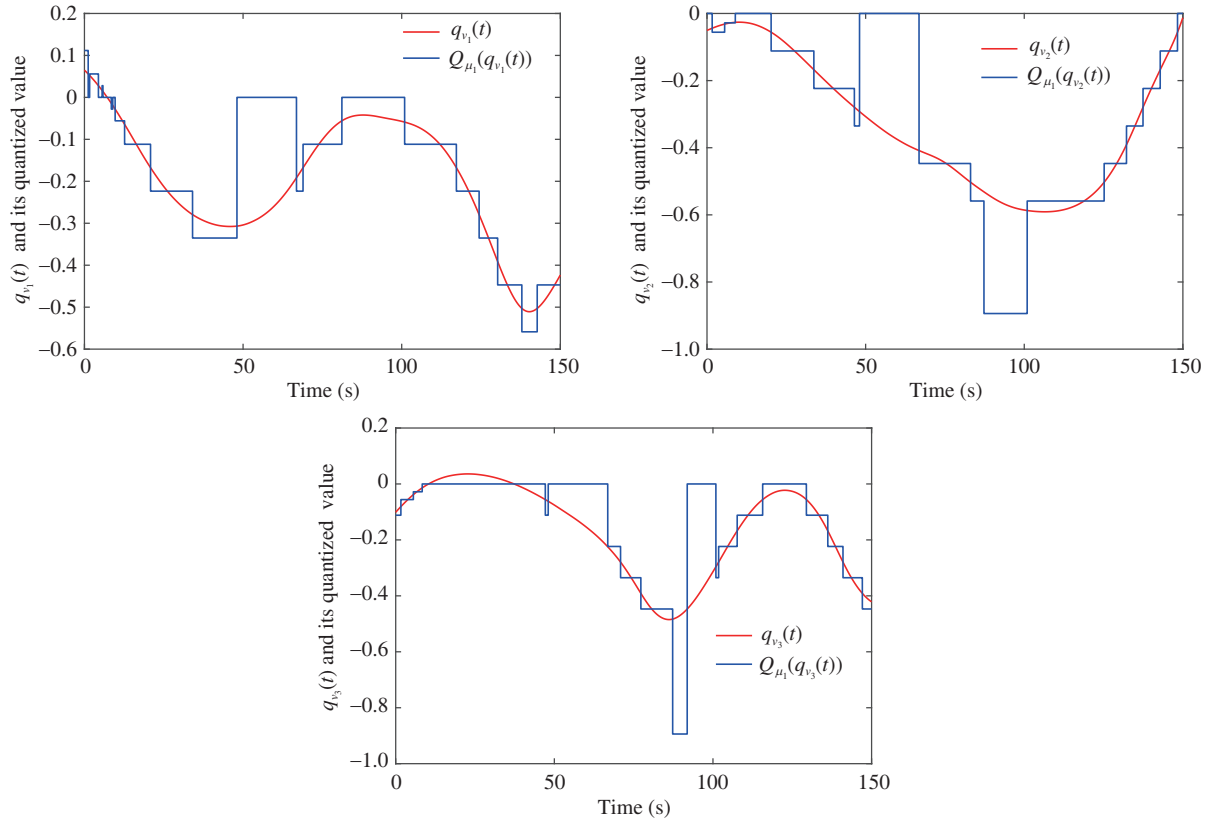
Figure 7 (Color online) Quaternion values and their quantized values under AFSMC.

4.3 Analysis of comparing experiments

From Figures 2 and 3, it can be seen that the proposed adaptive fuzzy backstepping controller can accommodate signal quantization and actuator faults effectively. However, from Figures 7 and 8, it is shown that the attitude variables diverge as time goes on, which means that the traditional AFSMC may not be qualified and cannot be directly applied when signal quantization and actuator faults exist. By the comparative experiments, it can be concluded that the proposed controller in this study has advantages over the traditional AFSMC when signal quantization and actuator faults exist, which endows the attitude control system more reliability against actuator faults, especially in application scenarios.
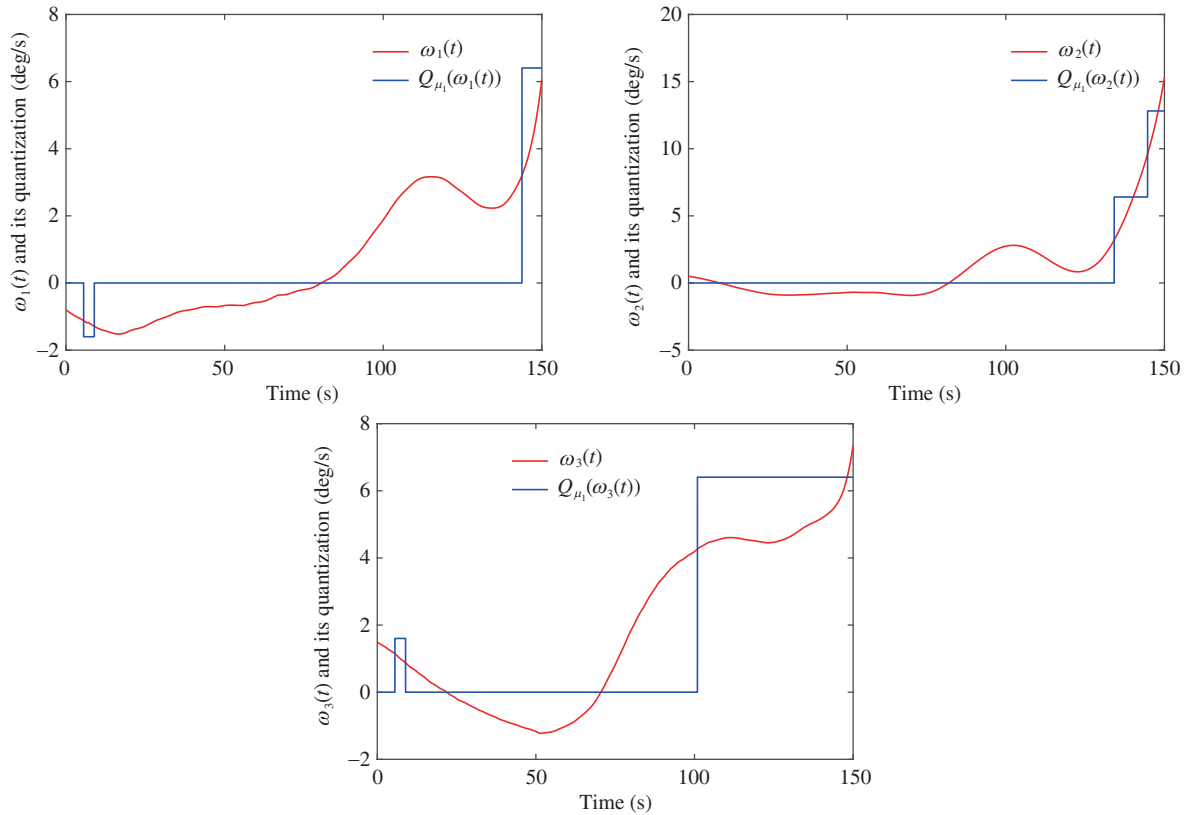
Figure 8 (Color online) Angular velocity values and their quantized values under AFSMC.

5 Conclusion

In this study, an adaptive fuzzy backstepping control strategy has been developed for flexible spacecraft systems with signal quantization and actuator faults. The proposed quantized fault-tolerant control strategy can effectively resolve the time-varying actuator failures, unmeasurable modal vibrations, and quantization errors simultaneously in case of a flexible spacecraft attitude control system by injecting the quantizer parameters into the controller gain and applying the backstepping design technique, the fuzzy logic method, and the adaptive estimation mechanism. Finally, the simulation results are compared to prove the effectiveness and advantages of the proposed control method. Future work will focus on the investigation of spacecraft control in the presence of signal quantization and communication delay.

References

1 Timmons K, Coderre K, Pratt W D, et al. The Orion spacecraft as a key element in a deep space gateway. In: Proceedings of IEEE Aerospace Conference, 2018

2 Nasir A, Atkins E M, Kolmanovsky I. Robust science-optimal spacecraft control for circular orbit missions. IEEE Trans Syst Man Cybern Syst, 2020, 50: 923–934

3 Meng D S, Liu H D, Li Y N, et al. Vibration suppression of a large flexible spacecraft for on-orbit operation. Sci China Inf Sci, 2017, 60: 050203

4 Sun L, Huo W. Adaptive fuzzy control of spacecraft proximity operations using hierarchical fuzzy systems. IEEE/ASME Trans Mechatron, 2016, 21: 1629–1640

5 McCamish S B, Romano M, Yun X. Autonomous distributed control of simultaneous multiple spacecraft proximity maneuvers. IEEE Trans Autom Sci Eng, 2010, 7: 630–644

6 Zou A M, de Ruiter A H J, Kumar K D. Distributed attitude synchronization control for a group of flexible spacecraft using only attitude measurements. Inf Sci, 2016, 343: 66–78

7 Huang P F, Lu Y B, Wang M, et al. Postcapture attitude takeover control of a partially failed spacecraft with parametric uncertainties. IEEE Trans Autom Sci Eng, 2019, 16: 919–930

8 Yin S, Xiao B, Ding S X, et al. A review on recent development of spacecraft attitude fault tolerant control system. IEEE Trans Ind Electron, 2016, 63: 3311–3320

9 Lu K F, Xia Y Q, Zhu Z, et al. Sliding mode attitude tracking of rigid spacecraft with disturbances. J Franklin Inst, 2012, 349: 413–440

10 Lu K F, Xia Y Q, Yu C M, et al. Finite-time tracking control of rigid spacecraft under actuator saturations and faults. IEEE Trans Autom Sci Eng, 2016, 13: 368–381

11 Sun L. Adaptive fault-tolerant constrained control of cooperative spacecraft rendezvous and docking. IEEE Trans Ind Electron, 2020, 67: 3107–3115

12 Qiao J Z, Li Z X, Xu J W, et al. Composite nonsingular terminal sliding mode attitude controller for spacecraft with actuator dynamics under matched and mismatched disturbances. IEEE Trans Ind Inf, 2020, 16: 1153–1162

13 Sun H B, Hou L L, Zong G D, et al. Fixed-time attitude tracking control for spacecraft with input quantization. IEEE Trans Aerosp Electron Syst, 2019, 55: 124–134

14 Zhang Z, Shi Y, Zhang Z X, et al. Modified order-reduction method for distributed control of multi-spacecraft networks with time-varying delays. IEEE Trans Control Netw Syst, 2018, 5: 79–92

15 Lyu J T, Qin J H, Ma Q C, et al. Finite-time attitude synchronisation for multiple spacecraft. IET Control Theory Appl, 2016, 41: 1106–1114

16 Chen T, Wen H, Wei Z T. Distributed attitude tracking for multiple flexible spacecraft described by partial differential equations. Acta Astronaut, 2019, 159: 637–645

17 Sun G H, Xu S D, Li Z. Finite-time fuzzy sampled-data control for nonlinear flexible spacecraft with stochastic actuator failures. IEEE Trans Ind Electron, 2017, 64: 3851–3861

18 Jiang B X, Lu J Q, Liu Y, et al. Periodic event-triggered adaptive control for attitude stabilization under input saturation. IEEE Trans Circ Syst I, 2020, 67: 249–258

19 Sun H B, Hou L L, Zong G D, et al. Composite anti-disturbance attitude and vibration control for flexible spacecraft. IET Control Theory Appl, 2017, 39: 2383–2390

20 Cao L, Xiao B, Golestani M, et al. Faster fixed-time control of flexible spacecraft attitude stabilization. IEEE Trans Ind Inf, 2020, 16: 1281–1290

21 Agarwal A, Vukovich G. Proportional-derivative-acceleration controller design for spacecraft with flexible appendages. Int J Space Sci Eng, 2019, 5: 123–137

22 Liu L, Liu Y J, Tong S. Neural networks-based adaptive finite-time fault-tolerant control for a class of strict-feedback switched nonlinear systems. IEEE Trans Cybern, 2019, 49: 2536–2545

23 Zhou Q, Du P H, Li H Y, et al. Adaptive fixed-time control of error-constrained pure-feedback interconnected nonlinear systems. IEEE Trans Syst Man Cybern Syst, 2020. doi: 10.1109/TSMC.2019.2961371

24 Zhao X M, Mo H, Yan K F, et al. Type-2 fuzzy control for driving state and behavioral decisions of unmanned vehicle. IEEE/CAA J Autom Sin, 2020, 7: 178–186

25 Yang X B, Zheng X L, Chen Y H. Position tracking control law for an electro-hydraulic servo system based on backstepping and extended differentiator. IEEE/ASME Trans Mechatron, 2018, 23: 132–140

26 Basin M V, Yu P, Shtessel Y B. Hypersonic missile adaptive sliding mode control using finite- and fixed-time observers. IEEE Trans Ind Electron, 2018, 65: 930–941

27 Pukdeboon C. Extended state observer-based third-order sliding mode finite-time attitude tracking controller for rigid spacecraft. Sci China Inf Sci, 2019, 62: 012206

28 Chen L H, Liu M, Huang X L, et al. Adaptive fuzzy sliding mode control for network-based nonlinear systems with actuator failures. IEEE Trans Fuzzy Syst, 2018, 26: 1311–1323

29 Ren Z, Cheng P, Shi L, et al. State estimation over delayed mutihop network. IEEE Trans Autom Control, 2018, 63: 3545–3550

30 Karimi H R, Gao H J. New delay-dependent exponential H_∞ synchronization for uncertain neural networks with mixed time delays. IEEE Trans Syst Man Cybern B, 2010, 40: 173–185

31 Yang Z Q, Cheng P, Chen J M. Learning-based jamming attack against low-duty-cycle networks. IEEE Trans Depend Secure Comput, 2017, 14: 650–663

32 Song X, Zheng W X. Linear estimation for discrete-time periodic systems with unknown measurement input and missing measurements. ISA Trans, 2019, 95: 164–172

33 Xia W, Zheng W X, Xu S. Event-triggered filter design for Markovian jump delay systems with nonlinear perturbation using quantized measurement. Int J Robust Nonlinear Control, 2019, 29: 4644–4664

34 Xu J J, Xu L, Xie L H, et al. Decentralized control for linear systems with multiple input channels. Sci China Inf Sci, 2019, 62: 052202

35 Jiang B P, Karimi H R, Kao Y G, et al. Reduced-order adaptive sliding mode control for nonlinear switching semi-Markovian jump delayed systems. Inf Sci, 2019, 477: 334–348

36 Huang C, Zhang X, Lam H K, et al. Synchronization analysis for nonlinear complex networks with reaction-diffusion terms using fuzzy-model-based approach. IEEE Trans Fuzzy Syst, 2020. doi: 10.1109/TFUZZ.2020.2974143

37 Zhu S Y, Liu Y, Lou Y J, et al. Stabilization of logical control networks: an event-triggered control approach. Sci China Inf Sci, 2020, 63: 112203

38 Zhou Q, Wang W, Ma H, et al. Event-triggered fuzzy adaptive containment control for nonlinear multi-agent systems with unknown Bouc-Wen hysteresis input. IEEE Trans Fuzzy Syst, 2019. doi: 10.1109/TFUZZ.2019.2961642

39 Wang W, Liang H J, Pan Y N, et al. Prescribed performance adaptive fuzzy containment control for nonlinear multiagent systems using disturbance observer. IEEE Trans Cybern, 2020, 50: 3879–3891

40 Chen Z Y, Han Q L, Yan Y M, et al. How often should one update control and estimation: review of networked triggering techniques. Sci China Inf Sci, 2020, 63: 150201

41 Su Y X, Wang Q L, Sun C Y. Self-triggered consensus control for linear multi-agent systems with input saturation. IEEE/CAA J Autom Sin, 2020, 7: 150–157

42 Ma H, Li H Y, Lu R Q, et al. Adaptive event-triggered control for a class of nonlinear systems with periodic disturbances. Sci China Inf Sci, 2020, 63: 150212

43 Cai D H, Zou H G, Wang J Z, et al. Event-triggered attitude tracking for rigid spacecraft. Sci China Inf Sci, 2019, 62: 222202

44 Lyke J C. Plug-and-play satellites. IEEE Spectr, 2012, 49: 36–42

45 Liu M, Zhang L X, Shi P, et al. Sliding mode control of continuous-time Markovian jump systems with digital data transmission. Automatica, 2017, 80: 200–209

46 Tong S C, Wang T, Li Y M. Fuzzy adaptive actuator failure compensation control of uncertain stochastic nonlinear systems with unmodeled dynamics. IEEE Trans Fuzzy Syst, 2014, 22: 563–574

47 Wang L X. Stable adaptive fuzzy control of nonlinear systems. IEEE Trans Fuzzy Syst, 1993, 1: 146–155

48 Cao X B, Yue C F, Liu M. Fault-tolerant sliding mode attitude tracking control for flexible spacecraft with disturbance and modeling uncertainty. Adv Mech Eng, 2017, 9: 1–9

49 Gao Z, Zhu Z H. Adaptive fast sliding model attitude tracking control for flexible spacecraft. In: Proceedings of the 4th International Conference on Control Science and Systems Engineering (ICCSSE), 2018. 264–268